Applied Medical Informatics
Original Research Vol. 42, No. 2 /2020, pp: 69-82

Automated Identification of Red Blood Cells in Optical Microscope Images of Blood Smears Using Various Color Segmentation Methods

Samer I. AWAD*, Rula G. ABDALLAT, Othman A. SMADI, Thakir D. ALMOMANI, and Salah M. ALZGHOUL

Department of Biomedical Engineering, Faculty of Engineering, The Hashemite University, P.O. Box 330127, Zarqa 13133, Jordan
E-mail(*): samer.awad@gmail.com

* Author to whom correspondence should be addressed; Tel.: ++962-797-695880.

Received: November 29, 2019 /Accepted: May 17, 2020/ Published online: June 30, 2020

Abstract
The identification and counting of red blood cells (RBCs) in microscopic blood images can provide useful information concerning the health of patients. Software-based cell counting has the advantages of objectivity, speed, and convenience over the manual method. Most of the automated RBC counting techniques in literature employed the grayscale or the green component of the red-green-blue (RGB) color images of blood smears. This work focuses on comparing the effect of using different color layers on the performance of software-based RBC counting. Ten color layers were extracted from different color models of blood smear images along with the grayscale conversion. Two comparisons were made: a comparison of contrast and a comparison of RBC counting performance using 52 blood smear images. The RBC contrast in the magenta layer of the cyan-magenta-yellow-key (CMYK) color model was at least 230% higher than that in the other layers. Additionally, our results indicated that using the magenta layer can provide better RBC counting performance when compared to the green, grayscale, and key layers with the p-values of $p=0.0283$, $p<0.0001$, and $p<0.0001$, respectively.

Keywords: Blood Cell Count; Erythrocytes; Optical Imaging; Image Processing, Computer-Assisted; Image Enhancement

Introduction

Blood contains three major cell types: erythrocytes or red blood cells (RBC), leukocytes or white blood cells (WBC), and thrombocytes or platelets. RBCs constitute about 45% of blood volume compared to about 55% for blood plasma [1, 2]. This hematocrit changes in the case of sickness, where the number of RBCs changes according to the type and severity of the disease. Hence, the assessment of RBC count is very important to detect as well as to follow up on the treatment of several diseases. A decrease in RBC count could indicate anemia, leukemia, or chronic inflammation [3, 4]. On the other hand, an increase in RBC count could indicate a poor heart function, poor lung function, or a renal tumor [3, 4].

RBC counting was conventionally implemented manually by a pathologist using an optical microscope. This method can be time-consuming (up to several minutes for each sample), subject to human error and interobserver variability, and dependent on the observer's skills. Nowadays, cell counting can be performed automatically using a hematology counter, which must be calibrated according to ranges specified by the manufacturer. However, hematology analysis is limited by the manufacturer's specifications, and it can be expensive [5-8]. Recently, hyperspectral imaging has been

successfully employed in automated RBC counting [9-12]. It integrates conventional imaging and spectroscopy technologies to obtain spatial and spectral information about the target. However, this method requires employing additional specialized equipment to implement the cell counting process (when compared to optical imaging), which increases the cost and complexity of the process.

Another automatic cell counting technique that is efficient (with relatively low false detections) and cost-effective (requires no additional equipment) is based on applying morphological image processing algorithms on optical microscope images of blood smears. A wide range of such algorithms has been developed to identify and count objects in blood smear color images [13-19].

Different methods can be used to represent a color image, known as color spaces or color models. RGB is a color model that consists of three layers: Red, Green, and Blue. HSV (Hue, Saturation, and Value) is an alternative representation of RGB. The CMYK model consists of four layers: Cyan, Magenta, Yellow, and Key (black). In each model, when the different layers are combined at different ratios, the whole spectrum of different visible colors can be created. RGB and HSV are characterized as additive color models, which mean layers are added to create a color image. In contrast, the CMYK model is characterized as a subtractive color model since the layers are subtracted.

Most automated cell counting methods that are based on image processing start with either isolating a color model layer or by converting the color image to grayscale. After color layer isolation, the following steps include threshold-based segmentation, cell identification (or classification), and cell counting [13, 15, 16, 18-20].

Several studies have suggested different methods for biological cell counting using different layers of blood color images. Safuan et al. employed color analysis of RGB, CMYK, and HSV color models, Otsu thresholding, and Circle Hough Transform for the segmentation and counting of WBCs with an average accuracy of 96.92% [13]. Romero-Rondón et al. proposed an algorithm based on Watershed transform for segmentation of overlapped RBCs using grayscale blood smear images that achieved sensitivity and specificity values of higher than 96% [15]. Tomari et al. presented an RBC counting analysis by considering an overlapping constraint using the green layer with an average accuracy of 83.5% [16]. Abbas also successfully employed the green layer for the automation of RBC counting using a histogram-based thresholding method [17]. Grayscale images were employed for the automatic detection of the malaria parasite in blood smear images layer with an average accuracy of 83.75% by Ghate et al. [21]. As for Putzu and Ruberto, they extracted the yellow layer of blood smear images and used it for the identification and counting of WBCs with an average accuracy of 92%. [22].

This study was carried out to investigate the effect of using different color layers on the performance of automated RBC counting including the ones presented in previous studies. The employment of the following layers was compared: red, green, and blue of the RGB color model, hue, saturation, and value of the HSV color model, and cyan, magenta, yellow, and key of the CMYK color model along with the grayscale image. The comparison was carried out by studying the contrast of RBCs in the images against the background and by evaluating the undercounting rate (UCR) and the overcounting rate (OCR) of RBC counting using the different layers.

Material and Method

Eleven color layers were studied: layers of the RGB, HSV, and CMYK color models along with the grayscale conversion of the original color image. The images used in this study (a total of 52 images of blood smears acquired from healthy subjects) were obtained from the Acute Lymphoblastic Leukemia Image Database for Image Processing (ALL-IDB) database [23]. The images were captured by using an optical microscope and a Canon PowerShot G5 camera. Figure 1 shows a sample blood smear color image along with the corresponding grayscale image and the RGB, HSV, and CMYK layers.

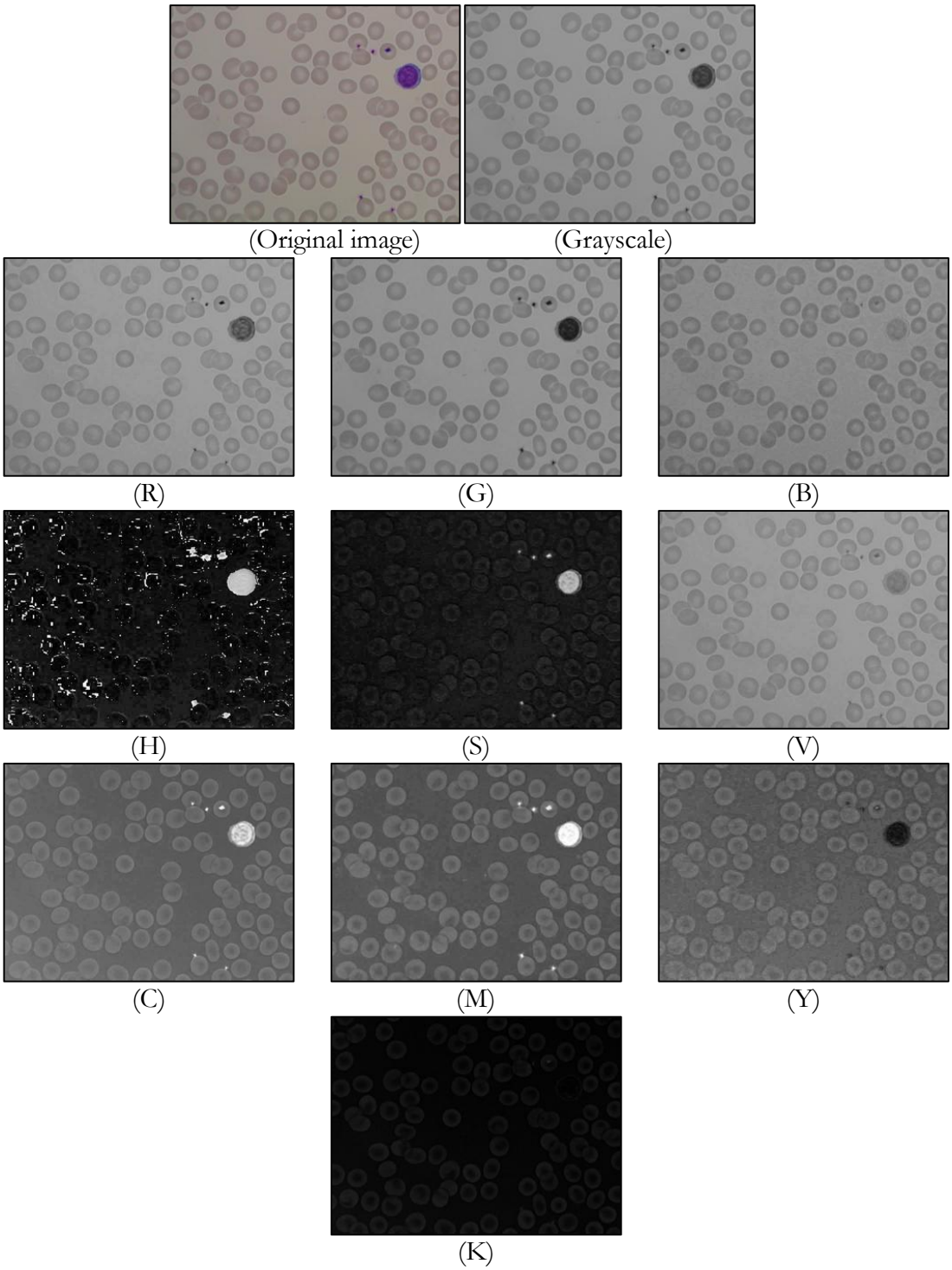

Figure 1. A sample blood smear color image (sample 27 as listed in Appendix (A), Table 2) along with the corresponding color layers: grayscale, red (R), green (G), blue (B), hue (H), saturation (S), value (V), cyan (C), magenta (M), yellow (Y), and key (K).

Contrast Calculations

In order to investigate the potential performance of RBC counting using different color layers, the contrast of RBCs was calculated. A total of nine images were selected for three different blood smears taken from three different subjects. In each image, four RBCs were selected to make a total of 36 contrast calculations. Calculations were done by extracting a chunk inside an RBC and

comparing it to a chunk from the background of the same size. The locations of the chunks were chosen visually for all cases. The chunks size was set to 4x4 μm² based on the typical RBC diameter of 6 to 8 μm. Figure 2 shows an example of how chunks were extracted for four contrast calculations. The following equation was used to calculate contrast values:

$$Contrast = \frac{|I_B - I_T|}{I_B + I_T} \quad (1)$$

where I_B is the average intensity of the background chunk, and I_T is the average intensity of the RBC chunk. To provide a measure for the dispersion of the contrast calculations, the standard deviation-to-mean ratios of the contrast values were also calculated.

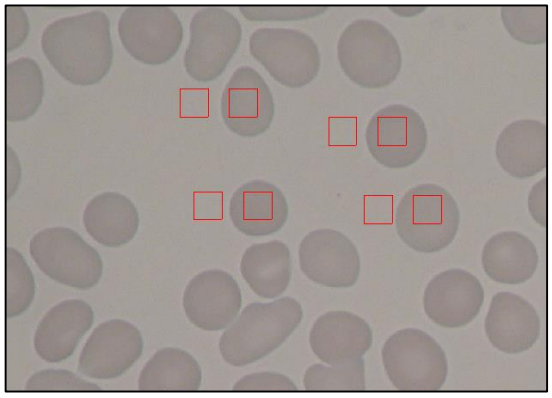

Figure 2. A sample blood smear image showing how the background and RBC chunks were extracted for four contrast calculations.

RBC Counting Framework:

Figure 3 presents the steps used in the framework of RBC identification and counting in this work.

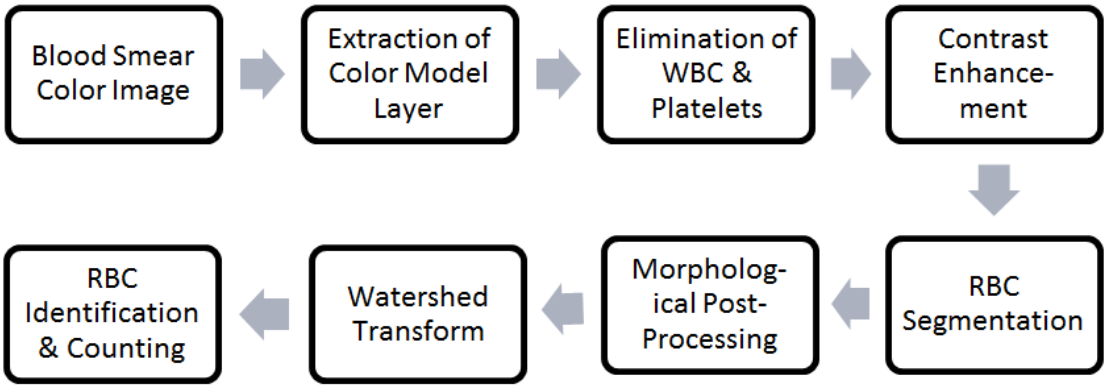

Figure 3. A flow chart showing the steps of RBC counting

Color Layer Extraction

RBC counting process starts with the extraction of a color model layer. All of the eleven layers shown in Figure 1 were investigated. The magenta layer of the blood smear sample used in Figure 1 was used to demonstrate the sequence of RBC counting steps (shown in Figure 4).

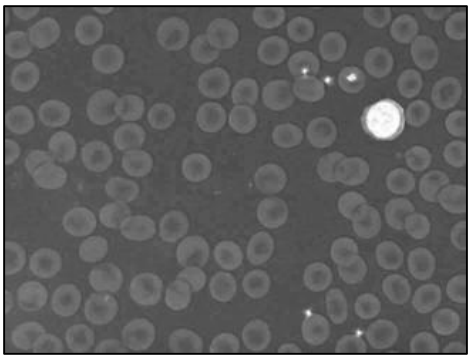

Figure 4. The magenta layer of a sample blood smear color image (sample 27 listed in Appendix (A), Table 2).

Elimination of WBCs and Platelets

By comparing the layers shown in Figure 1, the magenta layer shows the highest contrast for WBCs and platelets. Hence, this layer was used in this step. The layer was first converted to a binary image using Otsu's method (described below) to create a mask for the elimination of WBCs and platelets. Next, morphological dilation was applied to the mask in order to reduce any artifacts surrounding these cells. Circular dilation was used with a radius equal to 10% of the average of RBC radii in the image (assuming that RBCs are perfect circles). Figure 5 shows the WBCs and platelets mask along with the resulting image after masking.

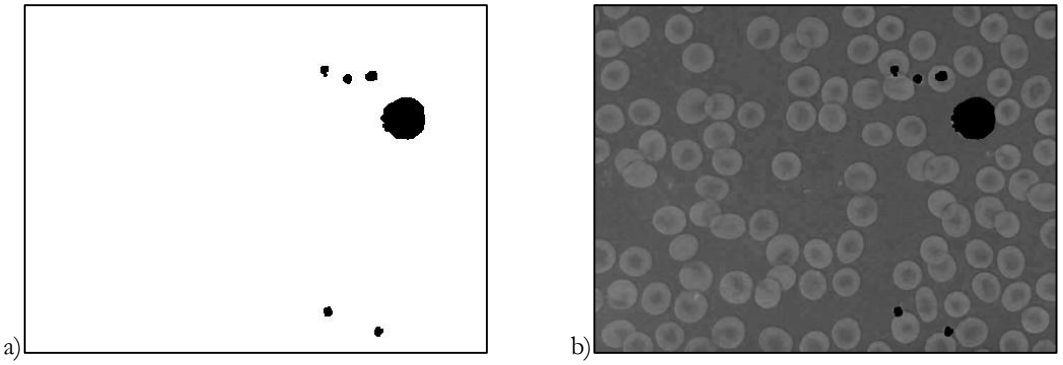

Figure 5. (a) The WBCs and platelets mask. (b) The resulting image after masking.

Contrast Enhancement

To make full use of the available dynamic range of brightness levels in a layer, contrast enhancement (or contrast stretching) was implemented [24]. This technique was implemented after the removal of WBCs and platelets presented in the previous step to stretch the histogram of the RBCs and the background without the presence of other cells. Consequently, more accurate RBC segmentation results can be achieved since the WBCs and platelets are not presented in the histogram of the image. Figure 6 shows the resulting image after contrast enhancement.

RBC Segmentation

Segmentation is the process of dividing a grayscale image into two homogenous regions: objects of interest and the background. The overall performance of RBC counting is highly dependent on the ability to segment the RBCs accurately. It has been reported that for a uniform type of image like a blood image, threshold-based segmentation produces reliable performance [13, 15, 16]. In this work, Otsu thresholding was used for RBC segmentation [25-27]. This operation reduces the color layer in the previous step into a binary image. Figure 7 shows the result of Otsu thresholding of the image in the previous step. Figure 8 compares thresholding results for all of the 11 color layers.

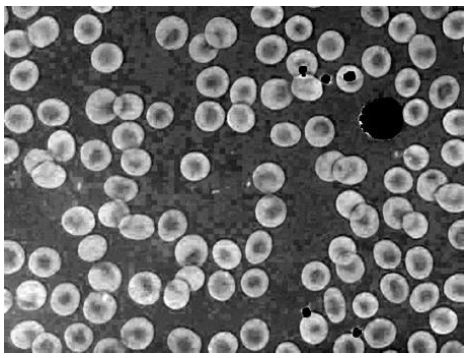

Figure 6. The resulting image after contrast enhancement

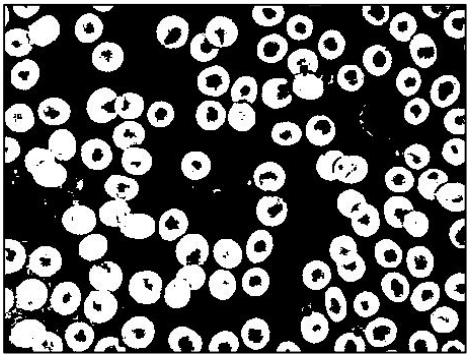

Figure 7. The binary image resulting from the thresholding of the image in the previous step

Morphological Post-Processing

Several unwanted artifacts can be noticed in Figure 7. In this step, several morphological operations are used to reduce these artifacts. Figure 9a shows the binary image after removing small objects. Holes inside the RBCs are artifacts caused by lighting and by the concave shape of the cells. These artifacts were reduced by using morphological closing. Additionally, morphological opening was implemented to reduce the irregularities at the edges of the detected objects. Both morphological closing and opening were implemented using a disk-shaped structuring element to preserve the circular nature of RBCs. The radius of the disk was 50% of the average of RBC radii in the image. Figures 9b and 9c show the binary image after implementing the morphological closing and opening, respectively.

Watershed Transform and Cell Counting

Some cells in blood smear images are clumped and overlapping (Figure 9c shows a few). In the cell counting step, several methods can be implemented to separate the overlapping cells including Circle Hough Transform [13, 18], edge detection [28], distance transform [29], and Watershed transform [15, 30].

In the Watershed transform (used in this work), a grayscale image is considered as a topographic surface, and the pixels with the highest gradient magnitude intensities correspond to watershed lines or boundaries that separate the objects that have to be segregated. To create these boundaries, markers or seeds have to be defined near the centers of these objects. To implement this, the Euclidean distance transform of the image in Figure 9c was first calculated (Figure 10a). For each pixel in a binary image, the distance transform calculates a number that is the distance between that pixel and the nearest nonzero pixel [31]. Next, the extended-minima transform was calculated, which estimates the local minima in a grayscale image [32]. This converts the result of the distance transform into an estimation of the centers of the objects in the binary image in Figure 9c which can be used as

watershed markers (Figure 10b). Watershed transform was next calculated and used to separate the overlapping cells (Figure 10c).

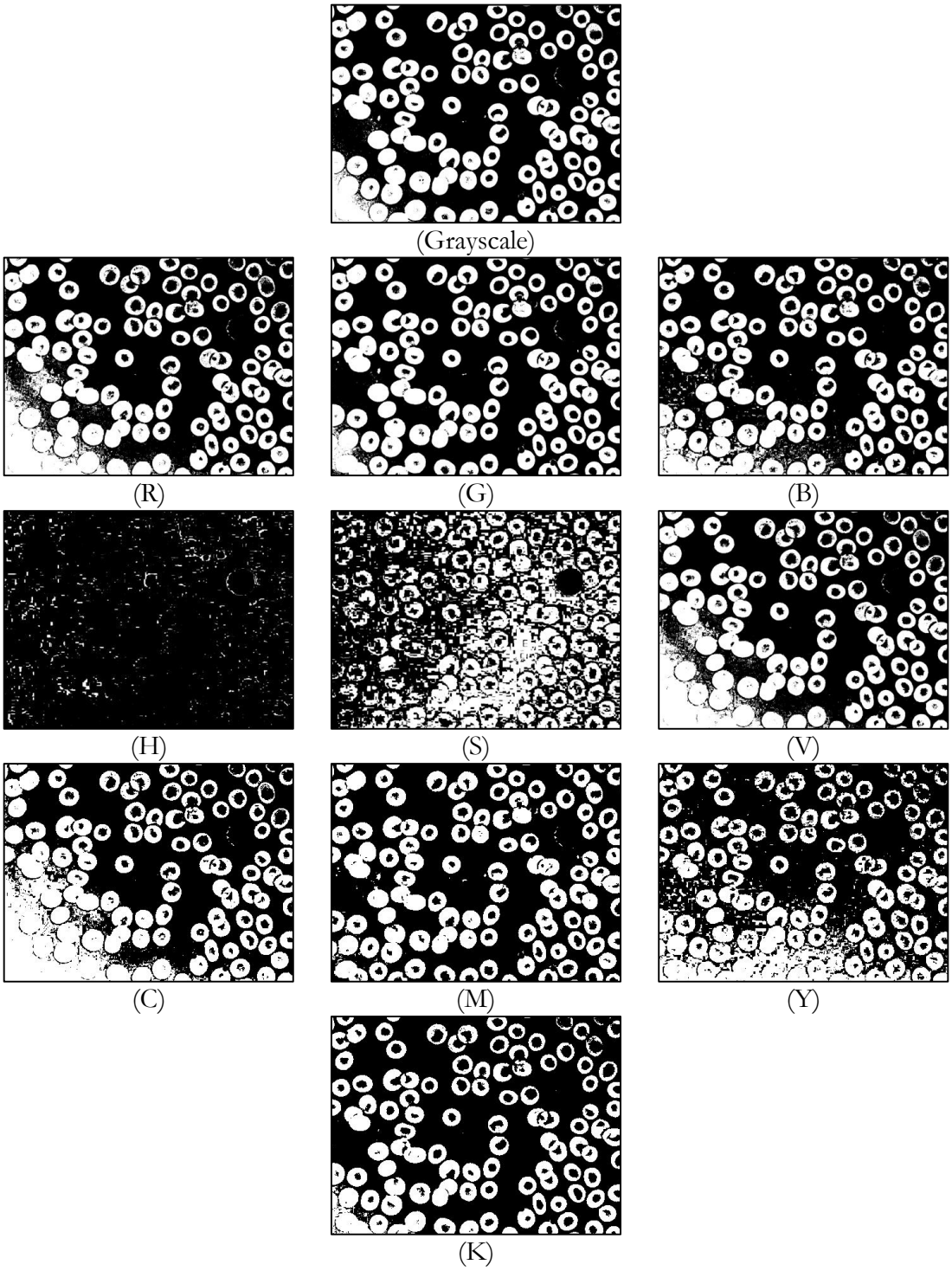

Figure 8. Otsu thresholding results of the blood smear sample used in Figure 1 for the color layers: grayscale, red (R), green (G), blue (B), hue (H), saturation (S), value (V), cyan (C), magenta (M), yellow (Y), and key (K).

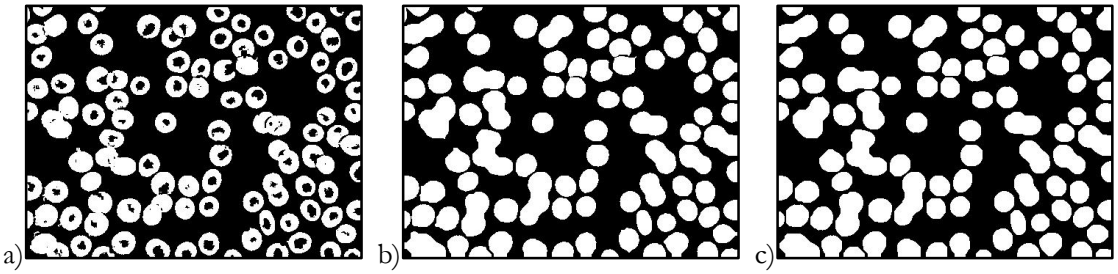

Figure 9. Morphological post-processing implemented on the image in Figure 5: (a) After removing small objects, (b) After morphological closing, (c) After morphological opening.

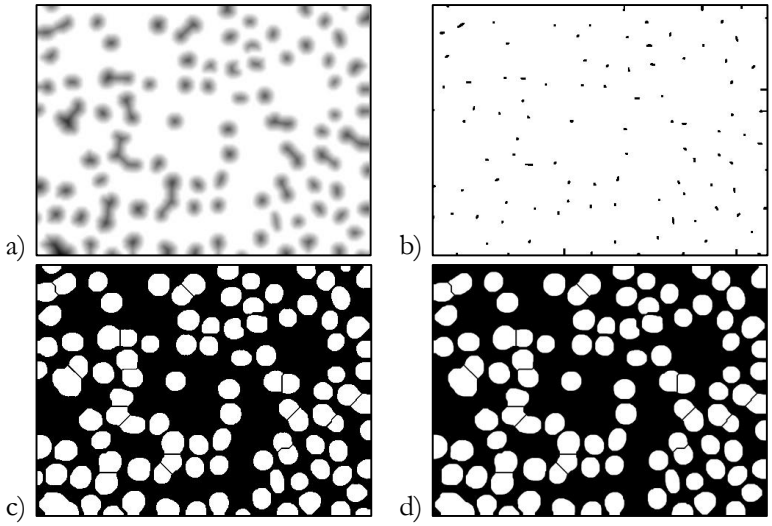

Figure 10. (a) Distance transform of the binary image in Figure 6c. (b) Extended-minima transform of the distance transform result. (c) The binary image after applying the watershed transform calculations. (d) The binary image after the removal of small and large objects.

Some large objects caused by false detections still appeared in the binary images at this stage (example: the bottom left object in the grayscale image in Figure 13). To remove such objects, the average object area in each image was calculated. Objects with areas larger than 200% of the average object area were removed. A common rule of thumb in manual RBC counting is to exclude cells at the edge of an image that have less than half of their area showing in the image. Objects at the edge of the binary image having an area less than 50% of the average object area were also removed. This gives the final result of RBC segmentation (Figure 10d) from which the RBC count was estimated.

Performance Evaluation

The cell counting technique described above was implemented on the 52 blood smear images mentioned above. To evaluate the performance of RBC counting, manual counting was implemented by a specialist using the color images to calculate the undercounting rate (UCR) and the overcounting rate (OCR) of the different layers. UCR and OCR can be defined as:

$$UCR = \frac{FN}{manual\ count} \quad (2)$$

$$OCR = \frac{FP}{manual\ count} \quad (3)$$

where FN (or false negatives) is the number of missed cells and FP (or false positives) is the number of falsely identified cells. Preliminary investigations showed that using magenta, green, grayscale and key outperformed the use the other color layers in RBC counting with an advantage for magenta.

Hence, cell counting was performed, and the UCR and OCR values were calculated, only for these four layers.

To test if there is a significant difference between the performance of cell counting using the magenta layer and the other three layers, unpaired t-test was carried out using Prism (Graphpad, San Diego, CA) for the UCR and OCR values (listed in Appendix (A), Table 2) achieved by using: magenta vs. green, magenta vs. grayscale, and magenta vs. key.

Results

Contrast Calculations

The averages of the 36 contrast calculations for the 11 color layers are presented in Figure 11. This figure shows high contrast average values for the hue, saturation, and key layers accompanied by high standard deviation values. Figure 12 shows the standard deviation-to-mean ratios of the contrast calculations. Table 1 in appendix (A) presents all the calculated contrast values.

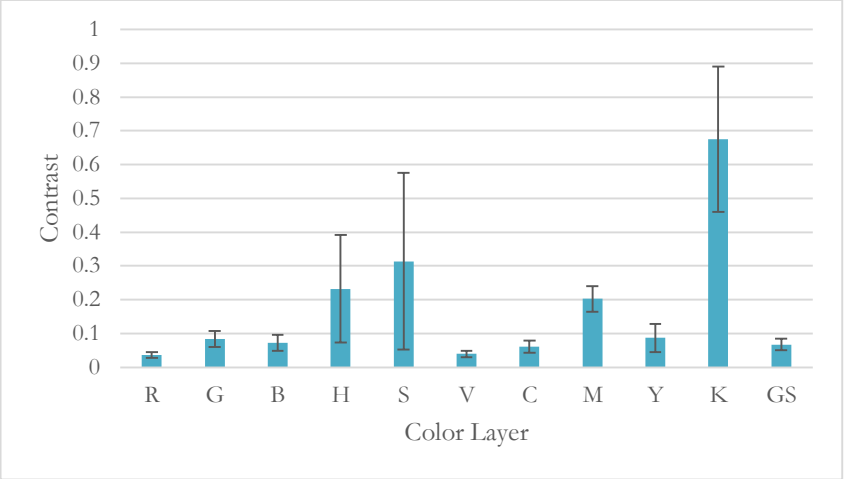

Figure 11. The average of the contrast values for the 11 color layers: red (R), green (G), blue (B), hue (H), saturation (S), value (V), cyan (C), magenta (M), yellow (Y), key (K), and grayscale (GS). The error bars shown represent plus and minus one standard deviation.

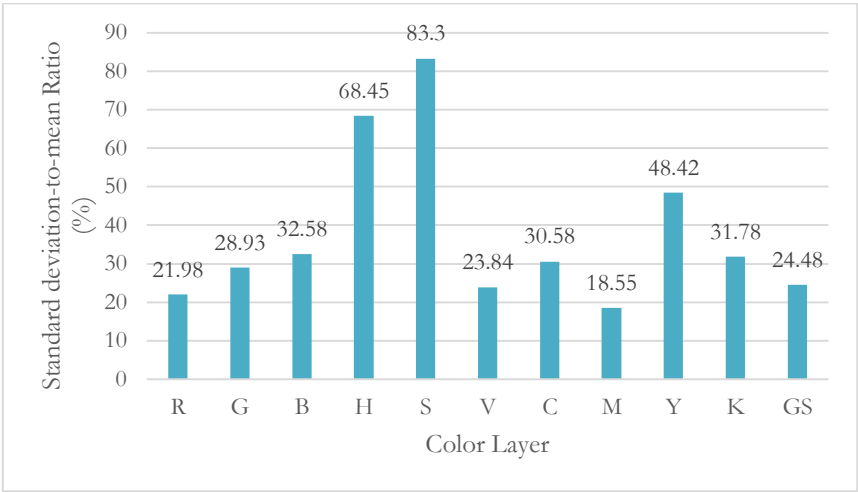

Figure 12. Standard deviation-to-mean ratios of contrast values for the 11 color layers: red (R), green (G), blue (B), hue (H), saturation (S), value (V), cyan (C), magenta (M), yellow (Y), key (K), and grayscale (GS).

RBC Counting and Performance Evaluation

To show the effect of using different color layers on RBC counting qualitatively, Figure 13 compares the result of RBC segmentation of blood smear sample used in Figure 1 after watershed transform and before removing small and large objects for the following color layers: magenta, green, grayscale, and key.

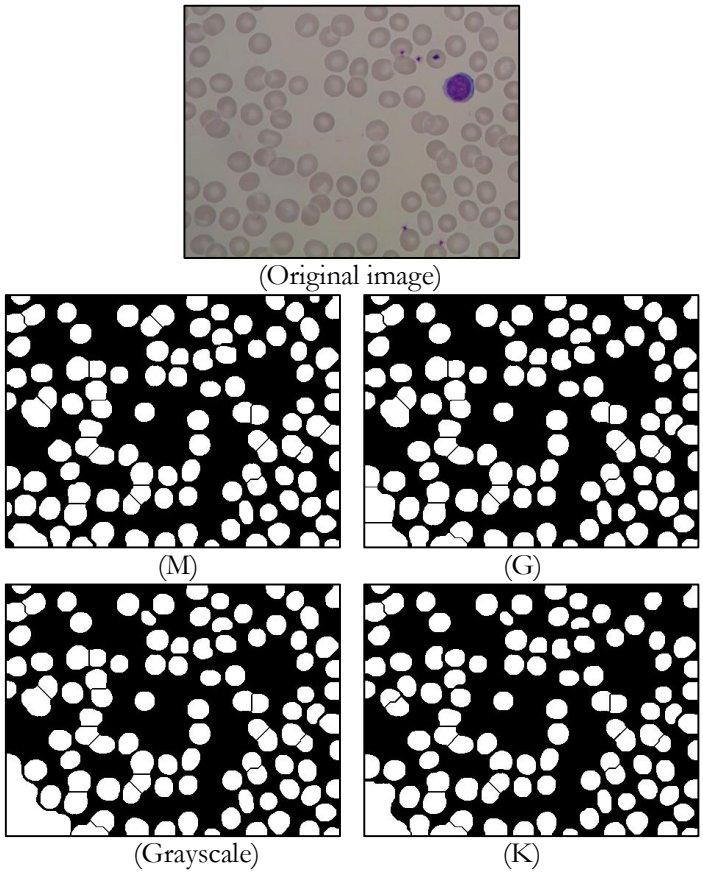

Figure 13. The result of RBC segmentation of the blood smear sample used in figure 1 after Watershed transform and before removing small and large objects for the following color layers: magenta layer (M), green layer (G), grayscale image, and key layer (K).

Quantitatively, Figure 14 present the average of UCR and OCR calculated by using the magenta, green, grayscale, and key layers for the 52 blood smear images. Table 2 in Appendix (A) presents the UCR and OCR calculations for all images.

Statistical analysis of the OCR and UCR values was implemented. The unpaired t-test analysis of the OCR values achieved by using: magenta vs. green, magenta vs. grayscale, and magenta vs. key resulted in the p-values of: $p= 0.4177$, $p=0.1161$, and $p=0.3486$, respectively. Image samples with UCR values of 10% or higher for all four methods were excluded from this analysis, which leaves 45 out of 52 cases (see Appendix (A), Table 2). Figure 15 compares the UCR values of the 45 images processed using the four methods. The unpaired t-test analysis of the UCR values achieved by using magenta vs. green, magenta vs. grayscale, and magenta vs. key resulted in the p-values of $p=0.0283$, $p<0.0001$, and $p<0.0001$, respectively. Figure 16 shows the final result of RBC segmentation using the magenta layer of three different blood smear samples.

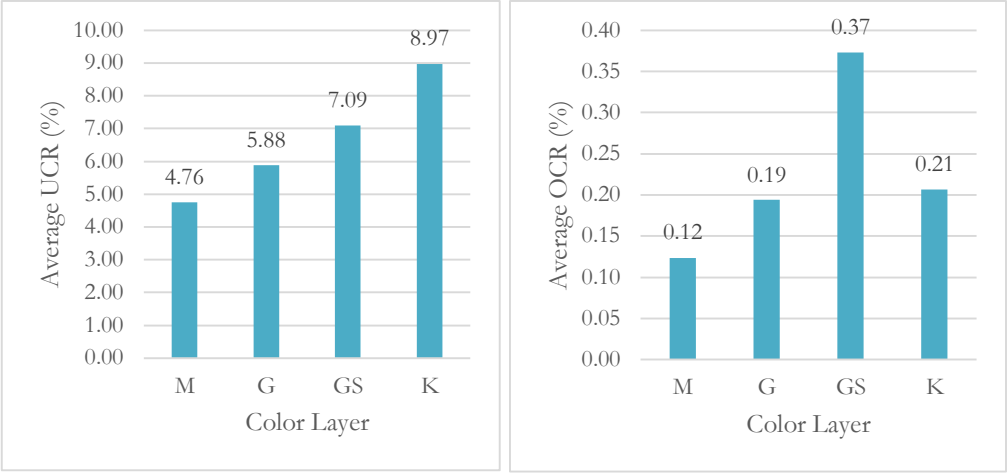

Figure 14. Average UCR and OCR calculated by using the magenta (M), green (G), grayscale (GS), and key (K) layers for the 52 blood smear images.

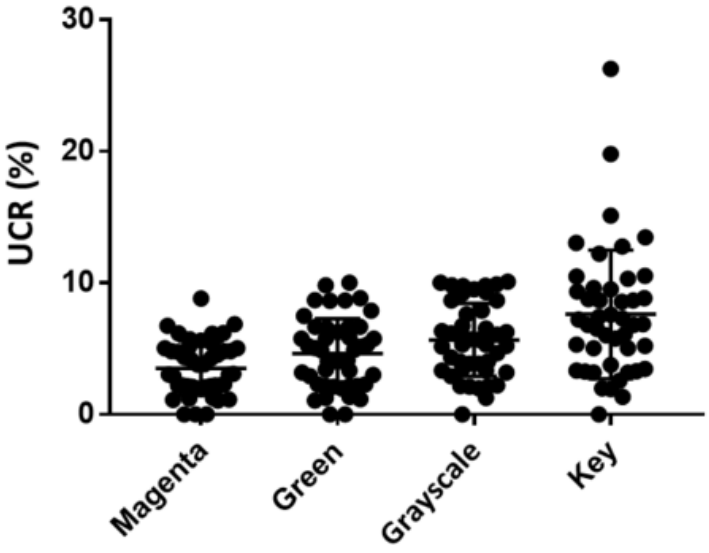

Figure 15. A comparison of the UCR values of the 45 images processed using the four color layers showing mean values and error bars that represent plus and minus one standard deviation.

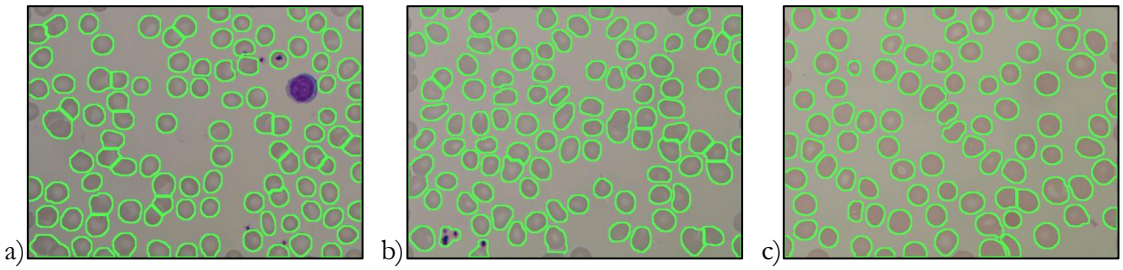

Figure 16. Result of RBC segmentation using magenta layer for: (a) Image 27 (as listed in Appendix (A), Table 2) with UCR = 4.81 and OCR = 0, (b) Image 8 with UCR = 5.05 and OCR = 2.02, and (c) Image 52 with UCR = 0 and OCR = 0.

Discussion

The comparison of average contrast values of RBCs using the 11 color layers shown in Figure 11 indicated that the hue, saturation, and key layers could provide better performance when used in RBC counting since they provide the highest contrast values. However, Figure 12 shows that the standard deviation-to-mean ratios for the hue and saturation layers are significantly high (around 68% and 83%, respectively). This fact correlates well with the morphological irregularities that can be seen in the hue and saturation images in Figure 1. It can also be noticed in Figure 11 that the contrast for the key layer is at least 200% higher than the contrast for the other layers. This is mainly due to the low average intensity in the key layer, which increases the contrast value since it is inversely proportional to the average intensity in an image. These observations indicate that the hue, saturation, and key layers can be unreliable to be used for RBC counting.

By ignoring the hue, saturation, and key layers and compare the average contrast values for the rest of the layers, it can be seen in Figure 11 that the value for the magenta layer is at least 230% higher than that for the other layers. Additionally, Figure 12 shows that the standard deviation-to-mean ratio of the magenta layer with the value of 18.55% is the lowest among all layers. This indicates that using the magenta layer can provide better performance for RBC counting compared to the use of the other color layers.

Preliminary investigations of RBC counting results showed that using magenta, green, grayscale and key outperformed the use the other color layers. RBC counting was implemented using these four layers and the UCR and OCR values were calculated. The average OCR calculated for the magenta layer was the lowest among the tested four layers with relatively small differences. However, the statistical analysis of the OCR values achieved by using the magenta layer showed insignificant advantage when compared to the green, grayscale, and key layers with p-values of larger than 11%. Comparing the average UCR values presented in Figure 14 shows that the four layers can be arranged according to performance (best to worst) in the following order: magenta, green, grayscale and key. The statistical analysis of the UCR values showed that the performance achieved by using the magenta layer can be significantly better than that for the other three layers with p-values of less than 3%. To assure robust results, Anova and nonparametric t-test, Fisher's pairwise comparisons, and two sample proportion test (p-test) were performed and showed consistent results. This also correlates well with the contrast investigation results and the qualitative comparison of images in Figures 1, 8, and 13.

Some hyperspectral imaging studies used UCR and OCR as measures of cell counting performance. Li et al. reported average UCR and OCR values of about 1.3% and 2.7%, respectively [9]. Liu et al. reported average UCR and OCR values of about 2.5% and 1.9%, respectively [10]. On the other hand, the performance evaluation of the method presented in this work using the magenta layer resulted in a comparable average UCR value of 4.76% and a less than one order of magnitude lower average OCR value of 0.16%

The number of false positives (estimated in the OCR calculations) in this study was very small when compared to the number of false negatives (estimated in the UCR calculations). Some false negatives were due to overlapping RBCs (see Figure 16a). These can be reduced by investigating the use of Hough transform or a combination of Hough transform and Watershed transform [13, 15]. Another cause for false negatives was cell fractions at the edges of blood smear images (see Figure 15). These can be reduced by investigating other methods for evaluating the area of cells at the edge of the image.

Future work will include evaluating the performance of using the magenta layer in RBC counting more rigorously using a larger image database and by using more false detection reduction techniques. The employment of the magenta layer in RBC counting will also be investigated along with the use of neural networks technique and color space correction using Lab color space [33]. Additionally, the employment of the magenta layer for the automated detection of other biological cells will be investigated.

Conflict of Interest

The authors declare that they have no conflict of interest.

References

1. Ganong WF, Barman SM, Barrett KE, Brooks HL, Boitano S. Ganong's review of medical physiology. 24th ed. New York: McGraw Hill Medical; 2012.
2. Almomani TD, Bani Hani S, Bdour A, Alsaraira AA, Smadi O, Al-Jarrah A, et al. Influence of erythrocyte shape on platelet scattering towards vessel wall. Int J Biomed Eng Technol. 2016;21(3):264–278. doi:10.1504/ijbet.2016.078289.
3. De Meyer T, De Buyzere ML, Langlois M, Rietzschel ER, Cassiman P, De Bacquer D, et al.. Lower red blood cell counts in middle-aged subjects with shorter peripheral blood leukocyte telomere length. Aging Cell 2008;7:700–705.
4. Wang Z, Song Z, Bai J, Li F, Hu J, Wu T, Qi J. Red blood cell count as an indicator of microvascular complications in Chinese patients with type 2 diabetes mellitus. Vasc Health Risk Manag. 2013;9:237–243. doi:10.2147/vhrm.s43211.
5. Estridge BH, Reynolds AP. Basic Clinical Laboratory Techniques. 6th ed. Delmar Cengage Learning; 2011.
6. Keohane E, Smith L, Walenga J. Rodak's Hematology: Clinical Principles and Applications. 5th ed. Saunders; 2015.
7. Cadena-Herrera D, Esparza-De Lara JE, Ramírez-Ibañez ND, López-Morales CA, Pérez NO, Flores-Ortiz LF, Medina-Rivero E. Validation of three viable-cell counting methods: Manual, semi-automated, and automated. Biotechnol Rep. 2015;7:9–16.
8. Sandhaus LM. Body Fluid Cell Counts by Automated Methods. Clin Lab Med. 2015;35(1):93–103.
9. Li Q, Zhou M, Liu H, Wang Y, & Guo F. Red Blood Cell Count Automation Using Microscopic Hyperspectral Imaging Technology. Appl Spectrosc. 2015;69(12):1372–1380.
10. Liu X, Zhou M, Qiu S, Sun L, Liu H, Li Q, & Wang Y. Adaptive and automatic red blood cell counting method based on microscopic hyperspectral imaging technology. J Optics. 2017;19(12):124014. doi:10.1088/2040-8986/aa95d7.
11. Conti M, Scanferlato R, Louka M, Sansone A, Marzetti C, & Ferreri C. Building up spectral libraries for mapping erythrocytes by hyperspectral dark field microscopy. Biomed Spectrosc Imaging 2016;5(2):175–184.
12. Lou J, Zhou M, Li Q, Yuan C, Liu H. An automatic red blood cell counting method based on spectral images. 9th International Congress on Image and Signal Processing, BioMedical Engineering and Informatics (CISP-BMEI). 2016, pp. 1391–1396. doi: 10.1109/CISP-BMEI.2016.7852934.
13. Safuan S, Tomari M, Zakaria W. White Blood Cell (WBC) Counting Analysis in Blood Smear Images Using Various Colour Segmentation Methods. Measurement 2017;116:543–555.
14. Elsalamony HA. Healthy and unhealthy red blood cell detection in human blood smears using neural networks. Micron 2016;83:32–41.
15. Romero-Rondón MF, Sanabria-Rosas LM, Mendoza-Castellanos A, Bautista-Rozo LX. Algorithm for detection of overlapped red blood cells in microscopic images of blood smears. Dyna 2016;83:188–195.
16. Tomari R, Zakaria W, Abdul Jamil M, Nor F, Fuad N. Computer Aided System for Red Blood Cell Classification in Blood Smear Image. Procedia Comput Sci. 2014;42:206–213.
17. Abbas S. Microscopic images data set for automation of RBCs counting. Data Brief 2015;5:35–40.
18. Maitra M, Gupta R, Mukherjee M. Detection and Counting of Red Blood Cells in Blood Cell Images using Hough Transform. Int J Comput Appl. 2012;53(16):13–17.
19. Khashman A. IBCIS: Intelligent blood cell identification system. Prog Nat Sci. 2008;18:1309–1314.

20. Awad SI, Abdallat R, Smadi O, AlMomani T. Automated Identification and Counting of Proliferating Mesenchymal Stem Cells in Bone Callus. Int J Comput Vis Robot. 2019;9(1):1-13. doi: 10.1504/IJCVR.2019.10016589.
21. Ghate D, Jadhav C, Rani N. Automatic Detection of Malaria Parasite From Blood Images. Int J Adv Comput Technol 2015;4(1):129–132.
22. Putzu L, Ruberto C. White Blood Cells Identification and Counting from Microscopic Blood Image. Int J Med Health Biomed Bioeng Pharm Eng. 2013;73:363–370.
23. Donida Labati R, Piuri V, Scotti F. ALL-IDB: the acute lymphoblastic leukemia image database for image processing. IEEE Int Conf on Image Processing (ICIP 2011), Brussels, Belgium. 2011, pp. 2045–2048.
24. Gonzalez RC, Woods RE. Digital Image Processing. 3rd ed. Pearson; 2007.
25. Feng Y, Zhao H, Li X, Zhang X, Li H.. A Multi-scale 3D Otsu Thresholding Algorithm for Medical Image Segmentation. Digit Signal Process. 2017;60:186–199.
26. Sezgin M, Sankur B. Survey over image thresholding techniques and quantitative performance evaluation. J Electron Imaging 2004;13(1):146–165.
27. Otsu N. A threshold selection method from gray-level histograms. IEEE Trans Sys Man Cyber. 1979;9(1):62–66.
28. Asmitaba G, Pipalia D. Design an Algorithm to Detect and Count Small Size Object Using Digital Image Processing. Int J Adv Res Elect Electron Instrument Eng. 2016;5(5):3807–3812.
29. Khan HA, Maruf GM. Counting Clustered Cells Using Distance Mapping. Int Conf Inform Electron Vis (ICIEV), Dhaka, Bangladesh. 2013, pp. 1–6.
30. Chourasiya S, Rani GU, Purushotham A. A Novel Automatic Red Blood Cell Counting System using Fuzzy C-Means Clustering. Int J Dig Appl Contemp Res. 2014;2(12):1–5.
31. Maurer, Calvin, Rensheng Qi, and Vijay Raghavan. A Linear Time Algorithm for Computing Exact Euclidean Distance Transforms of Binary Images in Arbitrary Dimensions. IEEE Trans Pattern Anal Mach Intell. 2003;25(2):265–270.
32. Soille P. Morphological Image Analysis: Principles and Applications. 1st ed. Springer-Verlag; 1999.
33. Reinhard E, Ashikihmin M, Gooch B, Shirley P. Color Transfer between Images. IEEE Comput Graph 2001;21(5):34–41.